remote sensing

MDPI

Article

Merging Alternate Remotely-Sensed Soil Moisture Retrievals Using a Non-Static Model Combination Approach

Seokhyeon Kim [1], Robert M. Parinussa [1], Yi Y. Liu [2], Fiona M. Johnson [1] and Ashish Sharma [1,*]

[1] School of Civil and Environmental Engineering, University of New South Wales, Sydney, NSW 2052, Australia; seokhyeon.kim@unsw.edu.au (S.K.); r.parinussa@unsw.edu.au (R.M.P.); f.johnson@unsw.edu.au (F.M.J.)

[2] Australian Research Council's Centre of Excellence for Climate Systems Science & Climate Change Research Centre, University of New South Wales, Sydney, NSW 2052, Australia; y.liu@unsw.edu.au

* Correspondence: a.sharma@unsw.edu.au; Tel.: +61-293-855-768

Academic Editors: Naser El-Sheimy, Zahra Lari, Adel Moussa, Nicolas Baghdadi and Prasad S. Thenkabail
Received: 19 March 2016; Accepted: 15 June 2016; Published: 21 June 2016

Abstract: Soil moisture is an important variable in the coupled hydrologic and climate system. In recent years, microwave-based soil moisture products have been shown to be a viable alternative to *in situ* measurements. A popular way to measure the performance of soil moisture products is to calculate the temporal correlation coefficient (R) against *in situ* measurements or other appropriate reference datasets. In this study, an existing linear combination method improving R was modified to allow for a non-static or nonstationary model combination as the basis for improving remotely-sensed surface soil moisture. Previous research had noted that two soil moisture products retrieved using the Japan Aerospace Exploration Agency (JAXA) and Land Parameter Retrieval Model (LPRM) algorithms from the same Advanced Microwave Scanning Radiometer 2 (AMSR2) sensor are spatially complementary in terms of R against a suitable reference over a fixed period. Accordingly, a linear combination was proposed to maximize R using a set of spatially-varying, but temporally-fixed weights. Even though this approach showed promising results, there was room for further improvements, in particular using non-static or dynamic weights that take account of the time-varying nature of the combination algorithm being approximated. The dynamic weighting was achieved by using a moving window. A number of different window sizes was investigated. The optimal weighting factors were determined for the data lying within the moving window and then used to dynamically combine the two parent products. We show improved performance for the dynamically-combined product over the static linear combination. Generally, shorter time windows outperform the static approach, and a 60-day time window is suggested to be the optimum. Results were validated against *in situ* measurements collected from 124 stations over different continents. The mean R of the dynamically-combined products was found to be 0.57 and 0.62 for the cases using the European Centre for Medium-Range Weather Forecasts Reanalysis-Interim (ERA-Interim) and Modern-Era Retrospective Analysis for Research and Applications Land (MERRA-Land) reanalysis products as the reference, respectively, outperforming the statically-combined products (0.55 and 0.54).

Keywords: dynamic; correlation coefficients; linear combination; soil moisture; AMSR2; JAXA; LPRM

1. Introduction

Soil moisture plays an important role in the hydrological and climatological cycles [1,2]. As a viable alternative to *in situ* measurements of soil moisture, a number of microwave-based soil moisture retrieval algorithms and/or products have been developed [3–8] and used in various fields of Earth sciences [9,10]. Despite the global coverage of the passive microwave-based soil moisture products,

the coarse spatial resolution (>100 km^2) and the overall uncertainties in the products that result from the radiative transfer model [11] are some of the reasons why direct applications of these products has remained limited to date.

Accordingly, a number of studies for evaluating the soil moisture products have been carried out by comparing with *in situ* observations [12–15], inter-comparisons among the products [16,17] or other large-scale verification techniques [18–20]. Traditional verification is done using *in situ* observations, which are regarded as ground truth, with a range of metrics, such as bias, root mean square error, standard error and temporal correlation coefficient (R) used to summarize the performance of the products [21]. Among these metrics, R is used to characterize temporal dynamics because it is insensitive to bias. Because scaling approaches have been developed to adjust the dynamic range of soil moisture [22–24], the dynamic range of the two products being compared is not such an issue, and therefore, R is considered a suitable metric [25].

Accordingly, [26] proposed a strategy to improve R for satellite-derived soil moisture products by combining two different products having complementary strengths and weaknesses that cancelled out through the strategy used. The method was demonstrated with an application using the Advanced Microwave Scanning Radiometer 2 (AMSR2) products, retrieved by the Japan Aerospace Exploration Agency (JAXA) [6] and the Land Parameter Retrieval Model (LPRM) algorithm [7,27] respectively. The JAXA and LPRM algorithms share a common background in the radiative transfer model [28], but they apply different parameterizations for surface temperature, roughness and vegetation; and they also use different dielectric mixing models to convert the dielectric constant into soil moisture [21]. As a result, the performance of these two soil moisture products was found to be spatially complementary in terms of R against a reference soil moisture dataset. The approach of [26] was based on improving R against a selected reference over the entire period, through the implementation of pixel-based weight values resulting in a linear combination of the AMSR2 products. The rationale of the linear combination was to take the strengths of parent products resulting from semi-independent information. This can be accomplished by applying weights to each of the parent products and is effective when parent products are complementary.

This study is an extension of the previous combination scheme described in [26], and the main objective of this paper is to provide further improvements of the performance of the combination approach that was presented. We focus here on dynamic weights that take account of the time-varying performances of the different soil moisture products. The previous static combination uses the entire time series of data in order to calculate a single, constant weight for each point in space. The dynamic combination aims to use only a part of the time series, which has more useful information for representing temporal variability at a point in time. This has been shown to be successful in other applications; for example, [29] applied a time-varying weight for combining time series, which is the sum of the weight at the previous time step and an error following a Gaussian distribution. The work in [30] used time-varying error-based weights for combining river flows in arid areas. In addition, [31] combined five global sea surface temperature forecasts by applying seasonally-based weights. The contribution of this study is to use time-varying weights to maximize the correlation of soil moisture products against a chosen reference. A second aim of the study is to determine the optimal size of the time window to calculate the combination weights using data at a daily time step.

Datasets used in this study, as well as data preprocessing are described in Section 2. The methodology for the dynamic combination is presented in Section 3. In Section 4, results from the global experiments are presented, as well as further results from a simulation experiment. Finally, the combined products are compared against *in situ* observations. In Section 5, the results are summarized and discussed, and suggestions are put forward for future research.

2. Data and Processing

2.1. Data

2.1.1. Remotely-Sensed Soil Moisture Products

AMSR2 is the successor of the successful Advanced Microwave Scanning Radiometer for the Earth Observing System (AMSR-E, May 2002–October 2011) sensor and is a multi-frequency passive microwave radiometer mounted on the Global Change Observation Mission 1-Water (GCOM-W1) satellite. This satellite was launched by the JAXA in May 2012, and AMSR2 observations are available from July 2012 onwards. AMSR2 is observing in seven microwave frequencies in both vertical and horizontal polarization with a swath width of 1450 km, which results in a 2–3 day revisit time for a fixed point at the ground [32]. There are two AMSR2-based soil moisture products, retrieved by the JAXA and LPRM algorithms, and it was shown that the performance of the two products is spatially complementary, particularly in terms of R [26]. This complementary behaviour is the main driver of this study, as it suggests good results when linearly combining them. Here, we use the JAXA (ver. 1.0) and LPRM soil moisture products retrieved from the X-band 10.7-GHz brightness temperature, which is available from both algorithms. We are not limited to using the same frequency for both products when combining them. As it is known that night-time has more favourable conditions for soil moisture retrieval [33], only soil moisture products from descending overpasses (01:30 a.m. equatorial overpass time) were used. Finally, the study was done over a two-year study period (1 January 2013–31 December 2014). The additional data prior to and after the analysed period are used in the time windows for the dynamic combinations. All analyses were performed at the standard spatial resolution of 0.25° (approximately 25 km).

2.1.2. Reanalysis Soil Moisture Products

A reference soil moisture dataset is required in the combination approach described in [26], as well as in the next section of this paper and is assumed to represent ground truth and the target for combining the products. In this study, two different reanalysis products were used as the reference to determine the optimal window size globally, as well as to check the performance of the dynamic combination approach. The first reference product is the volumetric water content of the topmost layer (0–0.07 m) from the European Centre for Medium-Range Weather Forecasts Reanalysis-Interim (ERA-Interim, [34]). The second reference product is volumetric soil moisture content in the top layer (0–0.02 m) of the Modern-Era Retrospective Analysis for Research and Applications Land (MERRA-Land, [35]). Daily values at each grid cell were selected from the series of the reanalysis products. The selected value is the one that is temporally closest to the AMSR2 scan time over the grid on the day.

2.1.3. *In Situ* Soil Moisture Measurements and Ancillary Data

To independently evaluate the improvements in the combined product compared to the individual parent product, *in situ* measurements from the International Soil Moisture Network (ISMN, [36]) were used. The AMSR2 scan time was also applied to select daily observations that are closest to the AMSR2 observations.

To ensure that the *in situ* data are of high quality for validation, a number of checks and filters were used that required ancillary data. Firstly, ERA-Interim soil temperature in the top soil layer (0–0.07 m) was used to judge if a grid cell is frozen or not. Next, Topographic Complexity (TC) and Wetland Fraction (WF) data from the European Space Agency Climate Change Initiative (ESA CCI, [23,37,38]) were used to determine whether a ground station is an area representative for comparison with Remotely-Sensed (RS) soil moisture products. With this, the annual mean of vegetation optical depth (VOD) at 6.9 GHz derived from the LPRM algorithm was used as an indicator of vegetation density at each grid cell. The main characteristics of datasets used in this study are summarized along the data sources in Table 1.

Table 1. Details of datasets used in this study.

Data Source	Dataset	Temporal Resolution	Spatial Resolution	Units
AMSR2-JAXA	Level 3 geophysical parameter SMC	Daily	0.25°	m^3/m^3
AMSR2-LPRM	Level 3 Surface Soil Moisture X-band	Daily	0.25°	m^3/m^3
AMSR2-LPRM	Vegetation optical depth C-band	Daily	0.25°	-
AMSR2	Scan time	Daily	0.25°	s
ERA-Interim	Soil water contents Level 1 0–0.07-m depth	6 h	0.25°	m^3/m^3
ERA-Interim	Soil temperature Level 1 0–0.07-m depth	6 h	0.25°	K
MERRA-Land	Top soil layer soil moisture consent SFMC	Hourly	0.25° Resampled	m^3/m^3
ISMN	In situ measured soil moisture from 124 stations in 10 networks	Hourly	Point	m^3/m^3
ESA CCI	Topographic complexity, wetland fraction	-	0.25°	%

2.2. Data Preprocessing

A number of data preprocessing steps were applied to all of the remote sensing datasets, reanalysis and *in situ* observations. Firstly, a common procedure was adopted to exclude unreliable soil moisture retrievals from analyses [23,33]. Data under the following conditions was consistently masked, including: (1) grids contiguous to open water fluctuations, such as ocean or lakes; (2) densely-vegetated regions (annual mean of LPRM VOD at 6.9 GHz $\geqslant$0.8) where microwave radiation from the soil would be masked by the above lying canopy; and (3) frost conditions (soil temperature $\leqslant$273.15 K). The two algorithms treat the frozen conditions differently. The JAXA algorithm applies a fixed soil and vegetation physical temperature (293 K) [39], whereas the LPRM applies an internal scheme for masking such frozen conditions [7]. Accordingly, ERA-Interim soil temperature in the top soil layer (0–0.07 m) was consistently used to mask frozen conditions within the soil moisture products to ensure a good comparison.

Secondly, we adopted the following filtering criteria to minimize the systematic differences between RS products and point observations [40,41]. More details of the filtering methods can be found in [15]. (1) The shallowest measurement $\leqslant$10 cm was selected; (2) standard quality flags from the ISMN [42] were applied to remove spurious observations; (3) only stations in low wetlands and complex topography (WF and TC <10%) were selected; (4) areal representativeness of a station was considered. Such areal representativeness was determined through a cross comparison among the remote sensing, reanalysis and *in situ* data following [15]. When multiple stations exist in a grid, the station with the best areal representativeness was used for further analysis; (5) The Snow Telemetry (SNOTEL) and Atmospheric Radiation Measurement (ARM) networks were not used because their primary purposes are not soil moisture measurements [43], and only 40 stations from the Soil Climate Analysis Network (SCAN) were included for the comparison. The selected SCAN stations were used for the Soil Moisture and Ocean Salinity data assimilation experiments [44]; (6) Only *in situ* stations that have more than 100 paired observations with the RS products were included to ensure statistical robustness. As a result, 124 stations from 10 networks were used for the evaluation purposes, and their spatial distribution is presented in Figure 1. Even though we applied such strict filtering processes, it should be noted that there are likely to still be systematic differences among the datasets [45].

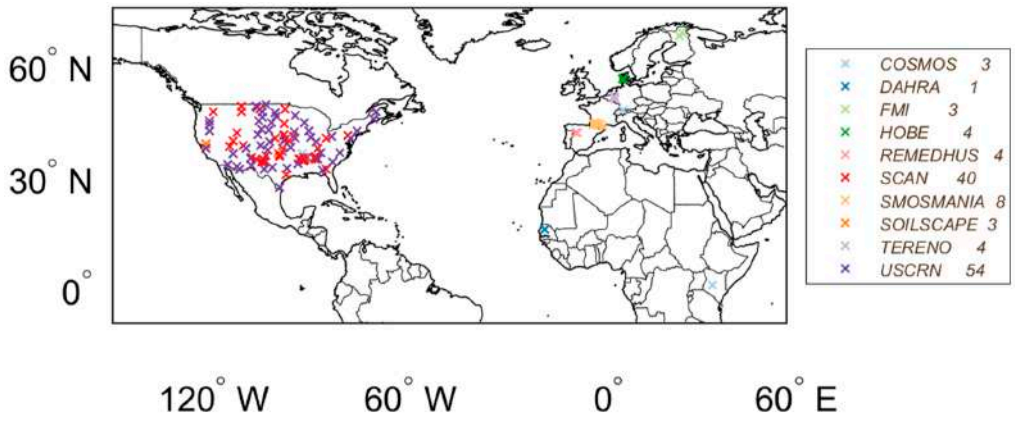

Figure 1. Locations of 124 ground stations from 10 networks used for the comparison with combined products.

3. Methodology

3.1. Static Linear Combination

The linear combination of forecasts was first introduced by [46] with the aim to minimize the mean square error from two parent forecasts. If one forecast uses information that the other has not considered, then the combined product is likely to take the strengths of each parent forecast and to have lower overall error. Since then, the linear combination has been widely used in diverse disciplines and improved for better performance [47–49]. Since the RS soil moisture products rely on different information and assumptions [21], the combination scheme was extended to soil moisture datasets to improve R [26]. Here, a summary of the previous linear combination is presented to show the potential for improvement. More details can be found in [26].

Two sets of unbiased soil moisture retrievals in a fixed time window are given as θ^1 and θ^2 (n × 1) and are linearly combined into θ^c by applying a single weight w (0–1).

$$\theta^c = w\theta^1 + (1 - w)\,\theta^2 \tag{1}$$

The Pearson correlation coefficient (R) between θ^c and a reference (θ^{Ref}) can be expressed as a function of w according to the definition of R and Equation (1), which is an optimization problem that can be described with the following equations.

$$\begin{array}{c} \text{Maximize } R = f(w) = \frac{E\left[\left(\theta^c - \mu^c\right)\left(\theta^{Ref} - \mu^{Ref}\right)\right]}{\sigma^c \sigma^{Ref}} \\ \text{Subject to } 0 \leqslant w \leqslant 1 \end{array} \tag{2}$$

where μ^c and μ^{Ref} are the mean values and σ^c and σ^{Ref} are the standard deviations of θ^c and θ^{Ref}, respectively. The work in [26] presents Equation (3) to calculate the optimal weight.

$$w = \frac{\sigma^2\left(R^{1\cdot Ref} - R^{1\cdot 2}\cdot R^{2\cdot Ref}\right)}{\sigma^1\left(R^{2\cdot Ref} - R^{1\cdot 2}\cdot R^{1\cdot Ref}\right) + \sigma^2\left(R^{1\cdot Ref} - R^{1\cdot 2}\cdot R^{2\cdot Ref}\right)} \tag{3}$$

where each σ presents the standard deviation of each product, and R is the temporal correlation coefficient between two products. It should be noted that Equation (3) is only applicable for two parent products that show positive temporal correlations against a reference, and the optimal weight is obtainable for general cases (*i.e.*, a pair of one or more products with negative and/or positive correlations against a reference) by solving the optimization problem described by Equation (2).

Despite the specificity of Equation (3), it provides important understanding of the linear combination approach maximizing R; (1) the optimal weight is mainly governed by temporal correlations among parent products and a reference; and (2) the optimal weight is influenced by

the ratio of standard deviations of the parent products. When there is a large disparity between the standard deviations of the parent products, Equation (3) is less influenced by the correlations when calculating the optimal weight, and it tends to converge to 0 or 1. Therefore, it is necessary to remove systematic differences among the datasets before applying the methodology. In this study, systematic differences were removed by a linear normalization using Equation (4) [45]; even though such a normalization approach assumes an equal noise level in the datasets, and therefore, the scaling coefficients and weight estimation are biased [24].

$$\theta^n = (\theta^r - \overline{\theta^r})\sigma^{Ref}/\sigma^r + \overline{\theta^{Ref}} \quad (4)$$

where θ^n normalized soil moisture, θ^r raw soil moisture, θ^{Ref} reference soil moisture, $\overline{\theta}$ mean of θ and σ standard deviation. With this, the only concern for the combination approach maximizing R is how parent products and a reference are different in terms of correlation coefficients.

Finally, the parent products (θ^1: JAXA; θ^2: LPRM) are combined through Equation (1) using the calculated the optimal weight at each grid cell. It should be further noted that this approach uses the entire dataset in a study period and calculates a set of constants as weights.

3.2. Dynamic Linear Combination

The existing static approach that uses the entire datasets to calculate the weights will be further developed by using a dynamic segment of the datasets instead. This is based on the premise that different data segments are affected in different respects resulting from the system state being measured. Hence, one can assume that if this state-dependent behaviour can be identified, combination weights may favour one retrieval algorithm over another for alternate states. This provides the basis for the dynamic combination approach presented here. The dynamic data segment is likely more dependent on and/or correlated with a spatiotemporal point to be combined and so is regarded to have more related information for calculating weights. For this, it is hypothesized that the information in a narrower range around the spatiotemporal point is more effective and sensitive for explaining temporal variability than the entire dataset. In this case, it is important to appropriately define the range of datasets by considering dimensional nearness to the point [50].

In this study, a temporally-moving window, which is cantered on the point of interest at time t and has a size N-days, is applied to define the temporal nearness. As presented in Figure 2, the dynamic linear combination uses a part of the datasets in a period T by the moving window, to calculate the optimal weight for the point in time t (w_t), and the linear combinations are successively performed at points in time by using the calculated time-varying weights.

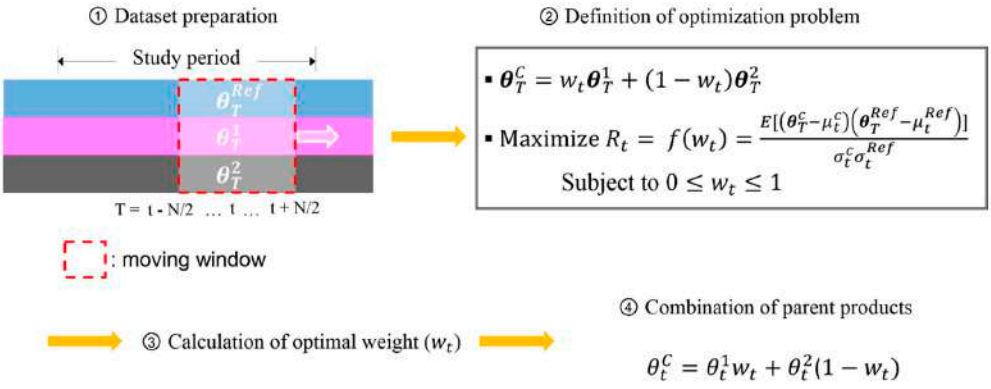

Figure 2. Schematic diagram for dynamic linear combination. T denotes the period defined by the window (*i.e.*, T = (t − N/2):(t + N/2)). Therefore, a bold symbol that has T as its subscript means a vector in the period T, and a non-bold symbol with t as the subscript represents a value at the point in time *t*.

4. Results

4.1. Global Data Combination with Various Scenarios

For most locations, time series of the AMSR2 products are generally not continuous over the seasons due to freezing conditions and the revisit pattern of AMSR2. This could directly result in a shortage of observations within a moving window leading to non-significant values of R. For this reason, a minimum number of observations is determined based on a two-tailed *t*-test with a significance level (α) for R.

$$t_{\alpha/2} = R \cdot \sqrt{\frac{n-2}{1-R^2}} \tag{5}$$

In this study, $\alpha = 0.05$, the corresponding $t_{\alpha/2} = t_{0.025} = 2.020$ and a target R = 0.4 are used, and the minimum number of observations (n) is determined to be 25. As it approximately needs 50–75 days for acquiring the minimum observations (*i.e.*, 25) due to the revisit time of AMSR2 (*i.e.*, 2–3 days), we set 60 as the minimum window size (N) for the dynamic combination.

Our initial experiment starts with using the volumetric water content of ERA-Interim as the assumed reference dataset. Both AMSR2 soil moisture products were then combined using the static combination and the dynamic combination with a range of window sizes (N = 60, 90 and 120 days). The combination results are presented in Figure 3a–f, which show global maps of R of the parent and combined products against the reference. Additionally, the box plot in Figure 3g shows the distributions of the global R for the various different scenarios (see Figure S1 in Supplementary Materials for results using MERRA-Land as the reference).

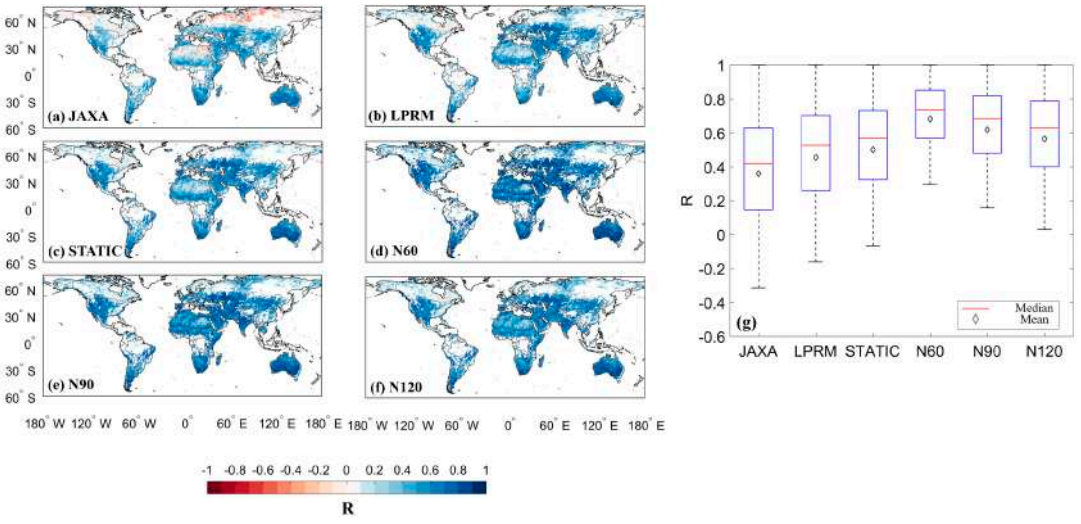

Figure 3. Results from experiments that uses ERA-Interim as the reference for various window sizes, N60, N90 and N120. Each panel shows the R between the reference and (**a**) JAXA; (**b**) LPRM; (**c**) static; (**d**) N60; (**e**) N90 and (**f**) N120; the more bluish colours in the maps indicate higher R against the reference; the overall performance for the various scenarios is summarized in the boxplot (**g**).

The spatial distributions of R tend to be improved (*i.e.*, more bluish colours) from the parent (Figure 3a,b) to statically- (Figure 3c) and dynamically-combined products (Figure 3d–f), and the tendency is clearly shown in the box plot of Figure 3g. The dynamically-combined products are consistently better than both parents and the statically-combined product. This result supports the hypothesis that data within a specific period provide better information for calculating weights maximizing R. It is also clear that the shorter window sizes in the dynamic combination outperform the longer window sizes. Hence, the N60 window size was selected for further analysis. To assess the sensitivity of this finding to the choice of reference dataset, this N60 scenario was again applied using

the top soil moisture layer of MERRA-Land as the reference dataset. Figure 4 presents the differences of this N60 experiment using ERA-Interim (top panels) and MERRA-Land (bottom panels) as the reference, respectively.

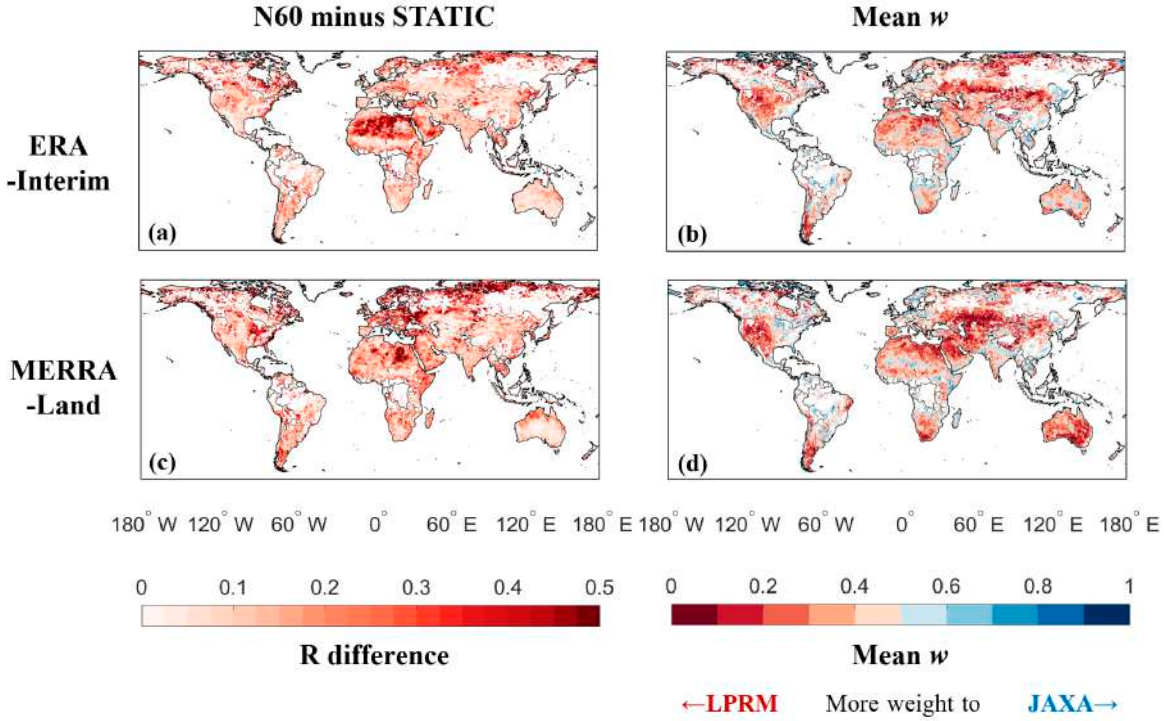

Figure 4. Comparison between combined soil moisture products. For ERA-Interim as the reference, (**a**) The differences in R between the static and N60 products against the reference (*i.e.*, R of N60 minus R of static) and (**b**) the mean weights that were used for the dynamic combination using the reference over the two-year study period; (**c**) and (**d**) show corresponding results with (**a**) and (**b**) when using MERRA-Land as the reference.

As shown in Figure 4a,c, the two dynamic products lead to improvements at different locations due to the different spatial patterns in agreement between each reference dataset and the parent products. As a result, the spatial distribution of the averaged weighting factors used for the dynamic combination is also different (Figure 4b,d). The differences are prominently contrasted over the desert regions, such as the Sahara, Middle East and central Australia. For comparison, results from the N90 and N120 are shown in Figures S2 and S3 in Supplementary Materials, and global maps are also presented in Figure S4 showing standard deviations of optimal weights from the two references (*i.e.* ERA-Interim and MERRA-Land) and three window sizes (*i.e.* N60, N90 and N120). To better understand these differences and how the chosen reference interacts with the parent products, we now setup an additional experiment in a controlled environment using simulated datasets.

4.2. A Simulation Experiment

To verify the results above, we assess the dynamic linear combination against the static approach in a simulation experiment that uses three periodical datasets generated by Equation (6).

$$\theta = A \cdot \sin(2\pi \cdot F \cdot \boldsymbol{t}) + M \tag{6}$$

where θ simulated soil moisture (m^3/m^3), A amplitude 0.2 (m^3/m^3), F frequency 1/365, $\boldsymbol{t}$ points in time (daily) and M mean soil moisture (0.4 m^3/m^3). The parameters used in Equation (6) are chosen for the simulated datasets to be within the plausible soil moisture range (0–0.6 m^3/m^3, [36]).

From the three generated datasets, two were designated as the parent products, and the remaining one was chosen to be the reference. To introduce different correlation coefficients among the parent products and the reference, which eventually govern the optimal weights, randomly-generated white noise from −0.2–+0.2 was added to each of the parent products. Next, an integer between 30 and 360 was also randomly selected for the size of moving window (N). After that, a series of dynamic combinations and a static combination were performed using data equivalent to a two-year period, and the correlations between the dynamically- (R_{dyn}) and statically- (R_{sta}) combined products were calculated and compared.

A correlation-based Euclidean distance was calculated for each simulation to represent the similarity/difference between the parent products and the reference. As there are two parent products for the combination, they are best summarized as a vector of the correlations, $(R_1, R_2)^T$, and then, the Euclidean distance (ξ) is calculated as follows.

$$\xi = \text{sqrt}((1 - R_1)^2 + (1 - R_2)^2) \quad (7)$$

Through this procedure, 1000 simulations were performed, and the results provide further information on the performance of the dynamic combination approach in terms of the window size (N) and also the influence on the results of the quality of the parent product(s).

The results from the simulation experiment show that: (1) the dynamic performance is consistently better than that of the static approach (Figure 5a); and (2) short window sizes provide the largest contrast between the static and dynamic approaches. Eventually, large window sizes will yield identical results as the static combination approach (Figure 5b). These results are in line with the results obtained through the global datasets, as was summarized in Figure 3. Figure 5a also shows that both performances tend to decrease with increasing Euclidean distance, in which the two linear regression lines imply strong dependence of both combination performances on initial quality of parent products.

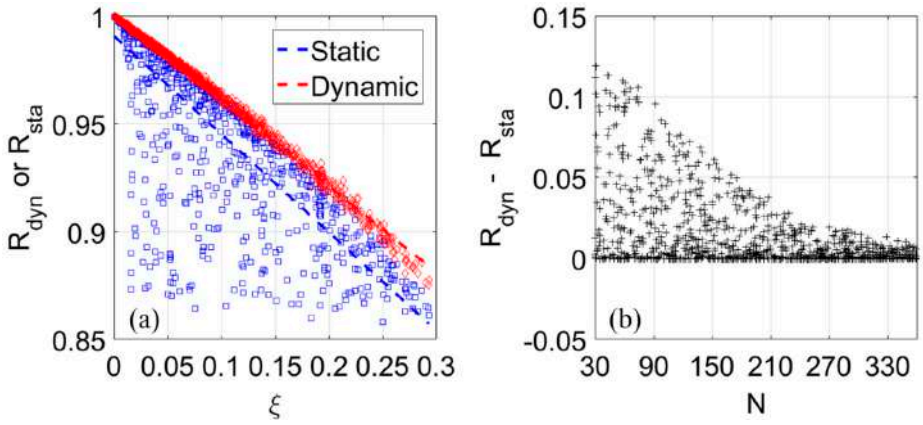

Figure 5. Results from the simulation experiment. (**a**) The x-axis indicates Euclidean distances (ξ) calculated by Equation (7), representing the qualities of the parent products, and the y-axis, R_{dyn} or R_{sta}. The dashed two lines present the linear regression of all results from the dynamic and static combinations, respectively; (**b**) The x-axis indicates N sizes, the y-axis differences between R_{dyn} and R_{sta} (*i.e.*, $R_{dyn} - R_{sta}$).

The final performance of the combination depends on the relative differences between the selected reference and the parent products. Therefore, an important consideration is that the quality of the combined product heavily relies on the quality of the reference that is assumed to represent the truth. Therefore, it is necessary to further investigate how the reference difference affects the combination performances from the static and dynamic approaches. In order to better understand the associated qualities of the different products, we compared them against *in situ* measurements from the ISMN.

4.3. Comparison against in Situ Observations

In this section, the dynamically-combined products with various scenarios are compared against *in situ* measurements from the ISMN. Through this comparison, we aim to demonstrate how much the results rely on the quality of the reference dataset. We present the R between the *in situ* measurements and the adopted reference dataset to demonstrate the impact of the R on the combination approach. For this comparison, the (N60) dynamic weighting approach was compared to the static weighting approach, as well as the parent products (Figure 6).

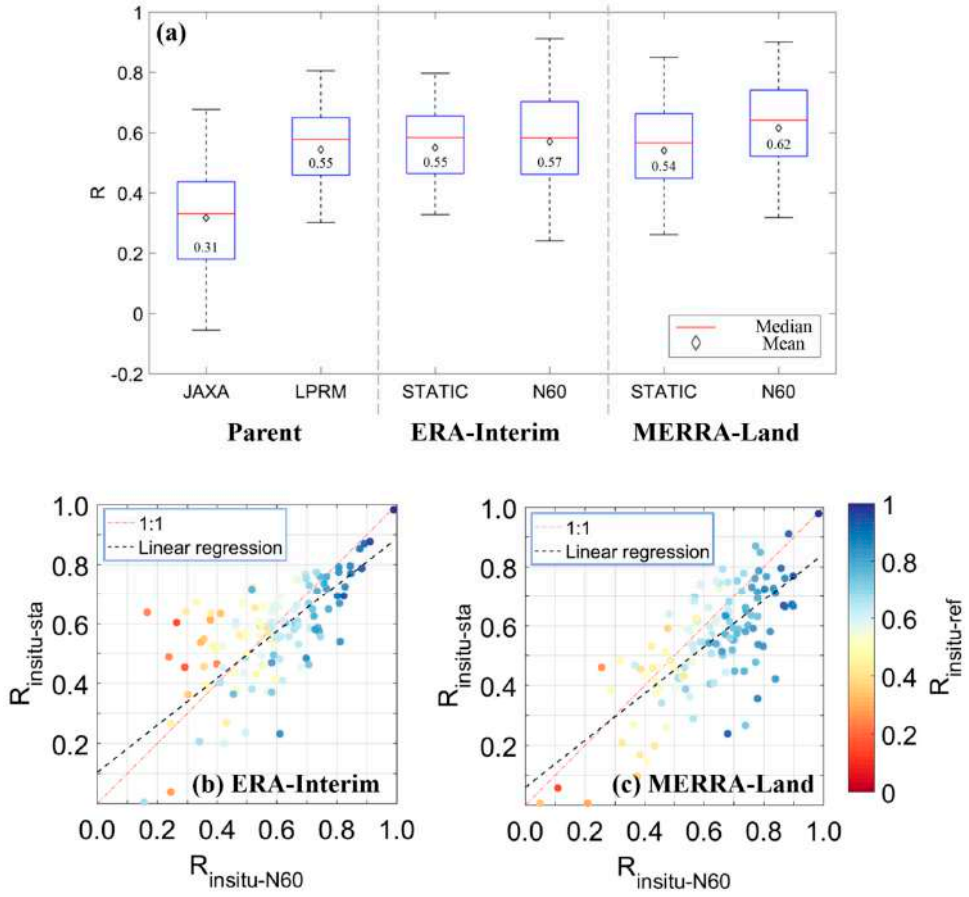

Figure 6. (**a**) Box plots showing combination performances against *in situ* measurements with the N60 and the two references. The labels on the x-axis indicate parent or statically-/dynamically-combined products with the references, and the y-axis R between the product and the *in situ* measurements. The value in each box is the mean of R. Comparison against *in situ* measurements from the ISMN for dynamically combined products using the N60 and (**b**) ERA-Interim and (**c**) MERRA-Land as the reference, respectively. The x-axis presents R between a dynamic product and the *in situ* measurements from a station, the y-axis R between a static product and the *in situ* measurements.

Data points in Figure 6 that are below the 1:1 line represent locations where the dynamic approach is better than the static one. The overall relation between these approaches over all sites in the ISMN is represented by the linear regression lines. Those regression lines show that the performance of the dynamic combination is generally better than the static approach, particularly when the initial R between the ISMN dataset and the reference data is high $R > 0.4$. An interesting feature obvious in Figure 6 is the qualitative differences in static and dynamic combination performances, where agreement between the reference and *in situ* measurements was expressed with colours from red to blue (0–1). The superiority in the dynamic approach is obvious when there is a better agreement between the reference and *in situ* measurements (bluish marks under the 1:1 line). However, degraded

performance for the dynamic approach is observed when the reference and *in situ* datasets do not agree (reddish marks above the 1:1 line). This suggests that the reference quality is important to consider when applying the dynamic approach. The dynamically-combined product tends to be closer to the reference; therefore, if the reference data are different from the *in situ* data, then the dynamic product will tend to deviate more from the *in situ* data, as well. In the case of ERA-Interim, the mean R of the static combinations is 0.55, which is similar to the LPRM product (0.55), but the dynamically-combined product (0.57) outperforms both parent products. For the case of MERRA-Land, the dynamic approach provides better performance (0.62) than the static approach (0.54) and all other products including the parent. From the results, it would be possible to select the static or dynamic product based on a threshold for the reference. In other words, it could be better to choose the static product if the reference quality is lower than the threshold or uncertain, which we further discuss in the next section.

As an example for the static and dynamic combination behaviour, Figure 7 is presented, which shows combination results using MERRA-Land as the reference at two ground stations where the dynamic approach outperforms most the static approach among the 124 stations.

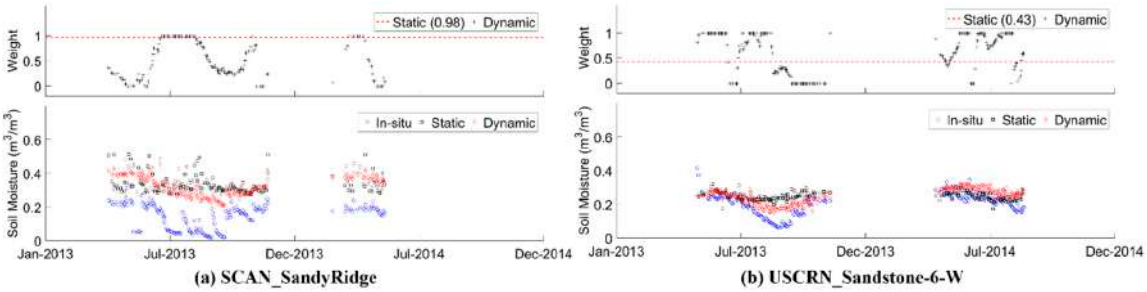

Figure 7. Dynamic and static combination results using MERRA-Land as the reference at (**a**) Sandy Ridge station in Soil Climate Analysis Network and (**b**) Sandstone-6-W station in U.S. Climate Reference Network. Each panel shows static/dynamic weights (**top**), as well as time series of statically- and dynamically-combined soil moisture products (**bottom**).

In the case of Sandy Ridge station (Figure 7a), the static weight is 0.98, and R between the statically-combined product and *in situ* measurements is 0.27. However, it sharply increases to 0.74 when applying the time-varying weights. For the case of Sandstone-6-W station (Figure 7a), the static weight is 0.43, and R between the statically-/dynamically-combined product and *in situ* measurements is 0.36 and 0.78, respectively.

4.4. Influence of the Quality of the Parent Products and Reference

The correlation-based Euclidean distance, used to assess the quality of the simulated datasets in Section 4.2, was extended to assess the quality of the parent products and reference against the in situ measurements.

Equation (7) is expanded to include three products (*i.e.*, two parent products and the reference dataset), and the vector of correlations at each station against *in situ* measurements is defined as $(R_{\text{insitu-JAXA}}, R_{\text{insitu-LPRM}}, R_{\text{insitu-ref}})^T$. Therefore, the extended Euclidean distance (ξ) is determined by:

$$\xi = \text{sqrt}(\left(1 - R_{insitu-JAXA}\right)^2 + \left(1 - R_{insitu-LPRM}\right)^2 + \left(1 - R_{insitu-ref}\right)^2) \quad (8)$$

At every station, R was determined through the static and dynamic approaches against corresponding *in situ* measurements ($R_{insitu-sta}$ and $R_{insitu-dyn}$) and was plotted against the Euclidean distances (Figure 8).

The dynamic approach shows generally better performances than the static approach, and this tendency is more conspicuous for MERRA-Land (Figure 8b) than for ERA-Interim (Figure 8a). It is also shown that $R_{insitu-sta}$ and $R_{insitu-dyn}$ tend to decrease with increases of ξ, which means that

a good agreement between the parent products and reference is an important precondition for both combination methods to provide improvements over the parent. As before, it is necessary to consider the quality of available reference datasets when deciding which one to use for these combination approaches.

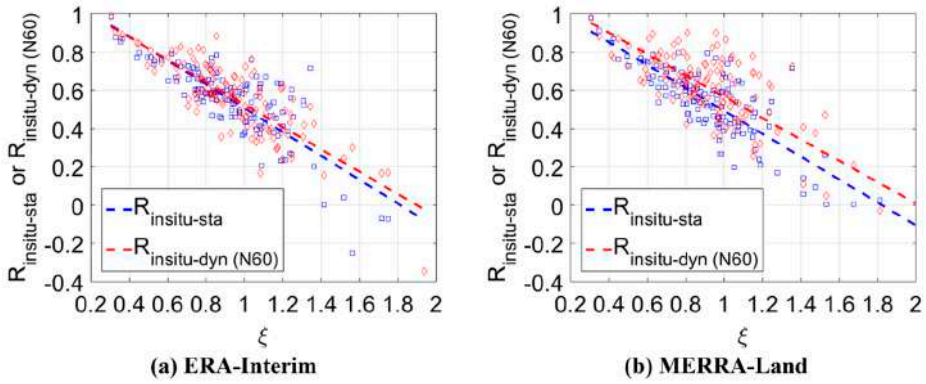

Figure 8. Combination performances with the quality of parent products and reference against *in situ* measurements. (**a**) ERA-Interim; (**b**) MERRA-Land. The x-axis for each panel presents the Euclidean distances (ξ) calculated by Equation (8), and the y-axis $R_{insitu-sta}$ or $R_{insitu-dyn}$. Linear regression lines represent the tendencies of both cases.

Figure 9 shows all $R_{insitu-sta}$ and $R_{insitu-dyn}$ from the two combination scenarios plotted against $R_{insitu-ref}$. The performance of the dynamic combination is clearly better than those of the static combination with higher $R_{insitu-ref}$. When $R_{insitu-ref}$ is around 0.6 or greater, then the dynamic combination is the superior approach. This suggests that a threshold value for $R_{insitu-ref}$ can be used to select when to use the dynamic or static combination approach. Namely, the static product is selected when $R_{insitu-ref}$ at a station is equal to or less than the threshold and vice versa, even though such approach can be only applied in areas where *in situ* measurements are available. That is to say, it can be optionally determined whether or not to apply the dynamic combination approach when a validation for the reference is supported. For example, [51] evaluated ERA-Interim soil moisture using *in situ* measurements from stations, and based on the results, one can have a basis for applying the static or dynamic combination approach over certain regions. In addition, the suggestion can be extended through large verification techniques, such as triple collocation [20].

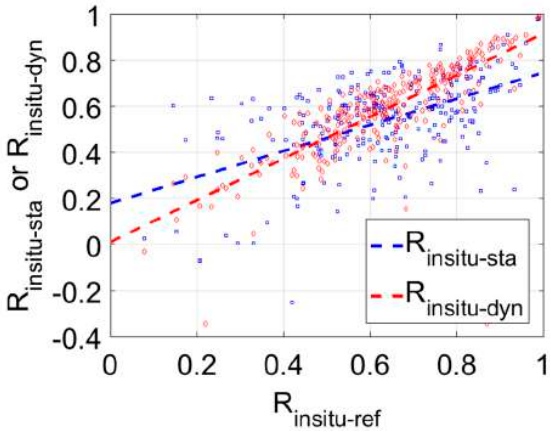

Figure 9. Combination performances with reference quality against *in situ* measurements. The x-axis presents R between *in situ* measurements and the references ($R_{insitu-ref}$), the y-axis R between *in situ* measurements and statically-/dynamically-combined products ($R_{insitu-sta}$ and $R_{insitu-dyn}$). Linear regression lines are added for representing the average tendencies of both cases.

5. Discussion

In this study, we present an approach to dynamically combine RS soil moisture products through a linear combination approach that maximizes R. The rationale of the proposed method is to use information from two parent products that are spatially and temporally complementary to each other. These parent products were linearly combined by applying a set of weights, which are governed by the correlation among the parent products and a used reference.

For this, it was hypothesized that datasets within a temporal moving window, cantered around a point in time and having size N, provide better information to calculate the optimal weight and lead to a better combination. Accordingly, it applied to the experiments using the two AMSR2 soil moisture products and the simulated datasets. The experiments led to three main conclusions about the dynamic combination methodology. (1) The dynamically-combined product is consistently better than the statically-combined and parent products when the reference quality is fairly good ($R > 0.6$); (2) better performances came out with shorter window sizes for the dynamic combination, and the N60 was selected as the optimum for combining these two AMSR2 products; (3) the performances of the dynamic and static approaches tend to decrease with the decreases of parent product quality against the reference.

In reality, the quality of a chosen reference is spatiotemporally variable [34,35], and this is likely to be the most important issue to be considered for combining parent products. To investigate this, experiments with two combination scenarios, the N60 with two references (*i.e.*, ERA-Interim and MERRA-Land), were performed and compared against the assumed truth, *i.e.*, *in situ* measurements from the ISMN. The results showed that the performance indeed relies on reference quality and a good quality of reference is essential for a good performance from the dynamic approach. We found that R between a reference and *in situ* data should be at least moderately positive (0.6). When the correlations are lower, the static combination is likely to be a more reliable choice based on the results from Figure 9.

6. Conclusions

Based on the results, there are a number of possibilities for future extensions. Firstly, the spatiotemporally-varying weights could provide information to improve the parent products, as well as the retrieval algorithms. The results here provide the JAXA and LPRM algorithms with clues on promising areas for further improvement by highlighting times of year and areas of the globe where the other product has superior performance. In addition, the results about the quality of the reference dataset highlight improvements that could be made in these products [51,52].

The combination scheme can be used with more than two parent products, so that it can reflect varying strengths resulting from the different techniques or retrieval algorithms. In this case, products from the same sensor but different frequencies or algorithms are preferred. This is because the products will then have the same swath pattern, leading to a good number of paired observations and the same scan time, so that the weather conditions are constant. A possible approach to combine multiple satellite-derived products from various sensors, which have different swath patterns and scanning times, is applying the methodology to datasets at coarser temporal resolutions (e.g., weekly) by averaging the original datasets at a finer temporal resolution. Lastly, it should be emphasized that the presented combination scheme is applicable to any spatiotemporal dataset where a reference dataset is available. From the results in this study, the following general guidelines are suggested for other applications of the dynamic linear combination. A minimum window size is recommended based on statistical significance to calculate the optimal weights. Secondly, the quality of a reference should be supported through a validation procedure to decide whether to accept or not the dynamically-combined product.

Supplementary Materials: The following are available online at www.mdpi.com/2072-4292/8/6/518/s1. Figure S1: Results from experiments that uses MERRA-Land as the reference for various window sizes (N60, N90 and N120). Each panel shows the R between the reference and (a) JAXA; (b) LPRM; (c) static; (d) N60; (e) N90 and (f) N120. The more bluish colors in the maps indicate higher R against the reference, the overall performance for the various scenarios is summarized in a boxplot (g). Figure S2: Differences in R between the static and dynamic products (N90 and N120). For ERA-Interim as the reference, (a) R of N90 minus R of static and (b) R of N120 minus R of static. (c) and (d) show corresponding results with (a) and (b) when using MERRA-Land as the reference. With relation to Figure 4a in the main manuscript, it is shown that the differences are more contrasted with shorter N sizes. Figure S3: Mean weights used for dynamically combined soil moisture products. For ERA-Interim as the reference, (a) presents mean weights from N90 over the 2-year study period, and (b) from N120. (c) and (d) show corresponding results with (a) and (b) when using MERRA-Land as the reference. Figure S4: Standard deviations of optimal weights used for dynamically combined soil moisture products. For ERA-Interim as the reference, (a) presents standard deviations from N60 over the 2-year study period, (b) from N90, and (c) N120. (d), (e) and (f) show corresponding results with (a), (b) and (c) when using MERRA-Land as the reference.

Acknowledgments: This work has been undertaken as part of a Discovery Project (DP140102394) funded by the Australian Research Council. Yi Liu is the recipient of an Australian Research Council Discovery Early Career Researcher Award Fellowship (DE140100200). Seokhyeon Kim is funded by a University of New South Wales Tuition Fee Scholarship (TFS). We are grateful to all contributors to the datasets used in this study. Particularly, we thank the teams from JAXA, Vrije Universiteit Amsterdam, European Centre for Medium-Range Weather Forecasts, Vienna University of Technology, NASA and all data contributors of the ISMN.

Author Contributions: Seokhyeon Kim initiated the study and did the analysis under the main supervision of Ashish Sharma. Robert M. Parinussa, Yi Y. Liu and Fiona M. Johnson provided regular feedback on the analysis and advised Seokhyeon Kim along the way. All authors contributed to the editing of the manuscript and to the discussion and interpretation of the results.

Conflicts of Interest: The authors declare no conflict of interest.

References

1. Koster, R.D.; Dirmeyer, P.A.; Guo, Z.; Bonan, G.; Chan, E.; Cox, P.; Gordon, C.; Kanae, S.; Kowalczyk, E.; Lawrence, D. Regions of strong coupling between soil moisture and precipitation. *Science* **2004**, *305*, 1138–1140. [CrossRef] [PubMed]
2. Taylor, C.M.; de Jeu, R.A.M.; Guichard, F.; Harris, P.P.; Dorigo, W.A. Afternoon rain more likely over drier soils. *Nature* **2012**, *489*, 423–426. [CrossRef] [PubMed]
3. Paloscia, S.; Macelloni, G.; Santi, E. Soil Moisture Estimates from AMSR-E Brightness Temperatures by Using a Dual-Frequency Algorithm. *IEEE Trans. Geosci. Remote Sens.* **2006**, *44*, 3135–3144. [CrossRef]
4. Akbar, R.; Moghaddam, M. A Combined active–passive soil moisture estimation algorithm with adaptive regularization in support of SMAP. *IEEE Trans. Geosci. Remote Sens.* **2014**, *53*, 3312–3324. [CrossRef]
5. Wagner, W.; Hahn, S.; Kidd, R.; Melzer, T.; Bartalis, Z.; Hasenauer, S.; Figa-Saldaña, J.; de Rosnay, P.; Jann, A.; Schneider, S. The ASCAT soil moisture product: A review of its specifications, validation results, and emerging applications. *Meteorol. Z.* **2013**, *22*, 5–33. [CrossRef]
6. Fujii, H.; Koike, T.; Imaoka, K. Improvement of the AMSR-E algorithm for soil moisture estimation by introducing a fractional vegetation coverage dataset derived from MODIS data. *J. Remote Sens. Soc. Jpn.* **2009**, *29*, 282–292.
7. Owe, M.; De Jeu, R.A.M.; Holmes, T. Multisensor historical climatology of satellite-derived global land surface moisture. *J. Geophys. Res. Earth Surf.* **2008**. [CrossRef]
8. Sandholt, I.; Rasmussen, K.; Andersen, J. A simple interpretation of the surface temperature/vegetation index space for assessment of surface moisture status. *Remote Sens. Environ.* **2002**, *79*, 213–224. [CrossRef]
9. Wagner, W.; Bloschl, G.; Pampaloni, P.; Calvet, J.-C.; Bizzarri, B.; Wigneron, J.-P.; Kerr, Y. Operational readiness of microwave remote sensing of soil moisture for hydrologic applications. *Nord. Hydrol.* **2007**, *38*, 1–20. [CrossRef]
10. Brocca, L.; Ciabatta, L.; Massari, C.; Moramarco, T.; Hahn, S.; Hasenauer, S.; Kidd, R.; Dorigo, W.; Wagner, W.; Levizzani, V. Soil as a natural rain gauge: Estimating global rainfall from satellite soil moisture data. *J. Geophys. Res. Atmos.* **2014**, *119*, 2014JD021489. [CrossRef]
11. Parinussa, R.M.; Meesters, A.G.C.A.; Liu, Y.; Dorigo, W.; Wagner, W.; De Jeu, R.A.M. Error estimates for near-real-time satellite soil moisture as derived from the land parameter retrieval model. *IEEE Geosci. Remote Sens. Lett.* **2011**, *8*, 779–783. [CrossRef]

12. Reichle, R.H.; Koster, R.D.; Liu, P.; Mahanama, S.P.P.; Njoku, E.G.; Owe, M. Comparison and assimilation of global soil moisture retrievals from the Advanced Microwave Scanning Radiometer for the Earth Observing System (AMSR-E) and the Scanning Multichannel Microwave Radiometer (SMMR). *J. Geophys. Res. Atmos.* **2007**. [CrossRef]
13. Brocca, L.; Melone, F.; Moramarco, T.; Wagner, W.; Hasenauer, S. ASCAT soil wetness index validation through *in situ* and modeled soil moisture data in central Italy. *Remote Sens. Environ.* **2010**, *114*, 2745–2755. [CrossRef]
14. Gruhier, C.; de Rosnay, P.; Hasenauer, S.; Holmes, T.; de Jeu, R.; Kerr, Y.; Mougin, E.; Njoku, E.; Timouk, F.; Wagner, W.; *et al.* Soil moisture active and passive microwave products: Intercomparison and evaluation over a Sahelian site. *Hydrol. Earth Syst. Sci.* **2010**, *14*, 141–156. [CrossRef]
15. Dorigo, W.A.; Gruber, A.; De Jeu, R.A.M.; Wagner, W.; Stacke, T.; Loew, A.; Albergel, C.; Brocca, L.; Chung, D.; Parinussa, R.M.; *et al.* Evaluation of the ESA CCI soil moisture product using ground-based observations. *Remote Sens. Environ.* **2015**, *162*, 380–395. [CrossRef]
16. Su, C.-H.; Ryu, D.; Young, R.I.; Western, A.W.; Wagner, W. Inter-comparison of microwave satellite soil moisture retrievals over the Murrumbidgee Basin, southeast Australia. *Remote Sens. Environ.* **2013**, *134*, 1–11. [CrossRef]
17. Rüdiger, C.; Calvet, J.-C.; Gruhier, C.; Holmes, T.R.; de Jeu, R.A.; Wagner, W. An intercomparison of ERS-Scat and AMSR-E soil moisture observations with model simulations over France. *J. Hydrometeorol.* **2009**, *10*, 431–447. [CrossRef]
18. Crow, W.T.; Miralles, D.G.; Cosh, M.H. A Quasi-Global Evaluation System for Satellite-Based Surface Soil Moisture Retrievals. *IEEE Trans. Geosci. Remote Sens.* **2010**, *48*, 2516–2527. [CrossRef]
19. Yilmaz, M.T.; Crow, W.T. Evaluation of Assumptions in Soil Moisture Triple Collocation Analysis. *J. Hydrometeorol.* **2014**, *15*, 1293–1302. [CrossRef]
20. Gruber, A.; Su, C.H.; Zwieback, S.; Crow, W.; Dorigo, W.; Wagner, W. Recent advances in (soil moisture) triple collocation analysis. *Int. J. Appl. Earth Obs. Geoinform.* **2016**, *45*, 200–211. [CrossRef]
21. Kim, S.; Liu, Y.Y.; Johnson, F.M.; Parinussa, R.M.; Sharma, A. A global comparison of alternate AMSR2 soil moisture products: Why do they differ? *Remote Sens. Environ.* **2015**, *161*, 43–62. [CrossRef]
22. Reichle, R.H.; Koster, R.D.; Dong, J.; Berg, A.A. Global Soil Moisture from Satellite Observations, Land Surface Models, and Ground Data: Implications for Data Assimilation. *J. Hydrometeorol.* **2004**, *5*, 430–442. [CrossRef]
23. Liu, Y.Y.; Parinussa, R.M.; Dorigo, W.A.; De Jeu, R.A.M.; Wagner, W.; van Dijk, A.I.J.M.; McCabe, M.F.; Evans, J.P. Developing an improved soil moisture dataset by blending passive and active microwave satellite-based retrievals. *Hydrol. Earth Syst. Sci.* **2011**, *15*, 425–436. [CrossRef]
24. Yilmaz, M.T.; Crow, W.T. The optimality of potential rescaling approaches in land data assimilation. *J. Hydrometeorol.* **2013**, *14*, 650–660. [CrossRef]
25. Entekhabi, D.; Reichle, R.H.; Koster, R.D.; Crow, W.T. Performance metrics for soil moisture retrievals and application requirements. *J. Hydrometeorol.* **2010**, *11*, 832–840. [CrossRef]
26. Kim, S.; Parinussa, R.M.; Liu, Y.Y.; Johnson, F.M.; Sharma, A. A framework for combining multiple soil moisture retrievals based on maximizing temporal correlation. *Geophys. Res. Lett.* **2015**, *42*, 6662–6670. [CrossRef]
27. Parinussa, R.M.; Holmes, T.R.H.; Wanders, N.; Dorigo, W.A.; de Jeu, R.A.M. A Preliminary Study toward Consistent Soil Moisture from AMSR2. *J. Hydrometeorol.* **2014**, *16*, 932–947. [CrossRef]
28. Mo, T.; Choudhury, B.J.; Schmugge, T.J.; Wang, J.R.; Jackson, T.J. A model for microwave emission from vegetation-covered fields. *J. Geophys. Res. Oceans* **1982**, *87*, 11229–11237. [CrossRef]
29. Terui, N.; van Dijk, H.K. Combined forecasts from linear and nonlinear time series models. *Int. J. Forecast.* **2002**, *18*, 421–438. [CrossRef]
30. Chowdhury, S.; Sharma, A. Multisite seasonal forecast of arid river flows using a dynamic model combination approach. *Water Resour. Res.* **2009**. [CrossRef]
31. Khan, M.Z.K.; Mehrotra, R.; Sharma, A.; Sankarasubramanian, A. Global Sea Surface Temperature Forecasts Using an Improved Multimodel Approach. *J. Clim.* **2014**, *27*, 3505–3515. [CrossRef]
32. Imaoka, K.; Kachi, M.; Kasahara, M.; Ito, N.; Nakagawa, K.; Oki, T. Instrument performance and calibration of AMSR-E and AMSR2. In *International Archives of the Photogrammetry, Remote Sensing and Special Information Science*; International Society of Photogrammetry and Remote Sensing: Kyoto, Japan, 2010.

33. De Jeu, R.A.M.; Wagner, W.; Holmes, T.R.H.; Dolman, A.J.; Giesen, N.C.; Friesen, J. Global Soil Moisture Patterns Observed by Space Borne Microwave Radiometers and Scatterometers. *Surv. Geophys.* **2008**, *29*, 399–420. [CrossRef]
34. Dee, D.P.; Uppala, S.M.; Simmons, A.J.; Berrisford, P.; Poli, P.; Kobayashi, S.; Andrae, U.; Balmaseda, M.A.; Balsamo, G.; Bauer, P.; *et al.* The ERA-Interim reanalysis: Configuration and performance of the data assimilation system. *Q. J. R. Meteorol. Soc.* **2011**, *137*, 553–597. [CrossRef]
35. Reichle, R.H.; Koster, R.D.; De Lannoy, G.J.M.; Forman, B.A.; Liu, Q.; Mahanama, S.P.P.; Touré, A. Assessment and Enhancement of MERRA Land Surface Hydrology Estimates. *J. Clim.* **2011**, *24*, 6322–6338. [CrossRef]
36. Dorigo, W.A.; Wagner, W.; Hohensinn, R.; Hahn, S.; Paulik, C.; Xaver, A.; Gruber, A.; Drusch, M.; Mecklenburg, S.; van Oevelen, P.; *et al.* The International Soil Moisture Network: A data hosting facility for global *in situ* soil moisture measurements. *Hydrol. Earth Syst. Sci.* **2011**, *15*, 1675–1698. [CrossRef]
37. Liu, Y.Y.; Dorigo, W.A.; Parinussa, R.M.; de Jeu, R.A.M.; Wagner, W.; McCabe, M.F.; Evans, J.P.; van Dijk, A.I.J.M. Trend-preserving blending of passive and active microwave soil moisture retrievals. *Remote Sens. Environ.* **2012**, *123*, 280–297. [CrossRef]
38. Wagner, W.; Dorigo, W.; de Jeu, R.; Fernandez, D.; Benveniste, J.; Haas, E.; Ertl, M. Fusion of active and passive microwave observations to create an essential climate variable data record on soil moisture. In Proceedings of the XXII ISPRS Congress, Melbourne, Australia, 25 August–1 September 2012; pp. 315–321.
39. Koike, T. Soil moisture algorithm. In *Descriptions of GCOM-W1 AMSR2 (Rev. A)*; Earth Observation Research Center, Japan Aerospace Exploration Agency: Tokyo, Japan, 2013; pp. 8–13.
40. Crow, W.T.; Berg, A.A.; Cosh, M.H.; Loew, A.; Mohanty, B.P.; Panciera, R.; de Rosnay, P.; Ryu, D.; Walker, J.P. Upscaling sparse ground-based soil moisture observations for the validation of coarse-resolution satellite soil moisture products. *Rev. Geophys.* **2012**. [CrossRef]
41. Gruber, A.; Dorigo, W.; Zwieback, S.; Xaver, A.; Wagner, W. Characterizing coarse-scale representativeness of *in situ* soil moisture measurements from the International Soil Moisture Network. *Vadose Zone J.* **2013**, *12*. [CrossRef]
42. Dorigo, W.A.; Xaver, A.; Vreugdenhil, M.; Gruber, A.; Hegyiová, A.; Sanchis-Dufau, A.D.; Zamojski, D.; Cordes, C.; Wagner, W.; Drusch, M. Global automated quality control of *in situ* soil moisture data from the International Soil Moisture Network. *Vadose Zone J.* **2013**, *12*. [CrossRef]
43. Dorigo, W.A.; Department of Geodesy and Geo-Information, Vienna University of Technology. Personal Communication, 2014.
44. De Lannoy, G.J.M.; Reichle, R.H. Global Assimilation of Multi-Angle and Multi-Polarization SMOS Brightness Temperature Observations into the GEOS-5 Catchment Land Surface Model for Soil Moisture Estimation. *J. Hydrometeorol.* **2015**. [CrossRef]
45. Draper, C.S.; Walker, J.P.; Steinle, P.J.; De Jeu, R.A.M.; Holmes, T.R.H. An evaluation of AMSR–E derived soil moisture over Australia. *Remote Sens. Environ.* **2009**, *113*, 703–710. [CrossRef]
46. Bates, J.M.; Granger, C.W. The combination of forecasts. *Oper. Res. Q.* **1969**, *20*, 451–468. [CrossRef]
47. Granger, C.W.J.; Ramanathan, R. Improved methods of combining forecasts. *J. Forecast.* **1984**, *3*, 197–204. [CrossRef]
48. Clemen, R.T. Combining forecasts: A review and annotated bibliography. *Int. J. Forecast.* **1989**, *5*, 559–583. [CrossRef]
49. Timmermann, A. Forecast Combinations. In *Handbook of Economic Forecasting*; Elliott, G., Timmermann, A., Eds.; Elsevier: Amsterdam, The Netherlands, 2006; Volume 1, pp. 135–196.
50. Sharma, A.; Mehrotra, R. An information theoretic alternative to model a natural system using observational information alone. *Water Resour. Res.* **2014**, *50*, 650–660. [CrossRef]
51. Albergel, C.; de Rosnay, P.; Balsamo, G.; Isaksen, L.; Muñoz-Sabater, J. Soil Moisture Analyses at ECMWF: Evaluation Using Global Ground-Based In Situ Observations. *J. Hydrometeorol.* **2012**, *13*, 1442–1460. [CrossRef]
52. Balsamo, G.; Albergel, C.; Beljaars, A.; Boussetta, S.; Brun, E.; Cloke, H.; Dee, D.; Dutra, E.; Muñoz-Sabater, J.; Pappenberger, F.; *et al.* ERA-Interim/Land: A global land surface reanalysis data set. *Hydrol. Earth Syst. Sci.* **2015**, *19*, 389–407. [CrossRef]